Chapter 4

Hot Wire Anemometry

4.1 Introduction

It was shown in Chapters 1 and 2 that there is a need for a better understanding of the unsteady loss mechanisms found in the high pressure turbine stage and that this is best achieved by making detailed experimental measurements of entropy at engine-representative conditions. Chapter 3 described the facility that has been used to simulate these conditions, whilst this Chapter and the next outline the necessary experimental techniques, which are based on the use of hot wire anemometry.

Hot wire anemometry has two main advantages over other measurement techniques that are relevant here. It is used in the aspirating probe, which is shown in Chapter 5 to be the only current means of measuring entropy accurately, and it can also be used to measure flow parameters very close to any end wall. Entropy was shown in Chapter 2 to be the only rational means of measuring loss, whilst near end wall measurements are vital in understanding the flow field in regions where the aspirating probe cannot be used due to its size. Hot wire anemometry is also a well-established, accurate and reliable technique with a high frequency response. This Chapter details the calibrations performed on the relevant hot wire probes as well as examining the general frequency response. This will allow the measurement accuracy to be estimated at any frequency, which is vital when analysing the experimental measurements presented in later Chapters.

4.2 Theory of operation

Fundamentally, a hot wire makes use of the principle of heat transfer from a heated surface being dependent upon the flow conditions passing over it. The self-explanatory mode of operation used here is Constant Temperature Anemometry (CTA), since it is widely available, is simple to use, and has a high frequency response, **Johnson, 1998**. To maintain the wire at a constant temperature a feedback circuit is used, Figure 4.2.1. The hot wire, shown between C and D, forms part of a Wheatstone bridge, such that the wire resistance is kept constant over the bandwidth of the feedback loop. Since the hot wire voltage is a simple potential division of the output voltage, the output voltage is normally measured for convenience.

Since the circuit response is heavily dependent upon the individual hot wire the feedback circuit must be tuned for each hot wire, **Dantec, 1986**. Although strictly it is necessary to test the hot wire with

velocity perturbations to optimise the frequency response, a much simpler electronic test has been developed that injects a small voltage square wave into the Wheatstone bridge. It has been shown by **Freymuth, 1977**, that the optimum circuit performance is found when the output response is approximately that shown in Figure 4.2.2. This allows the bandwidth to be estimated, although it has been shown by **Moss, 1992**, that any contamination of the wire reduces the frequency response without any apparent effect on the pulse response.

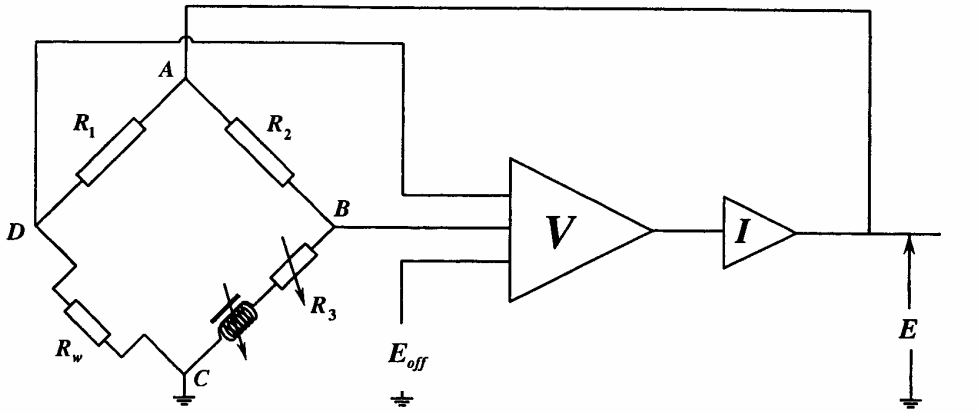

Figure 4.2.1 Schematic of a constant temperature anemometer, **Sheldrake, 1995**

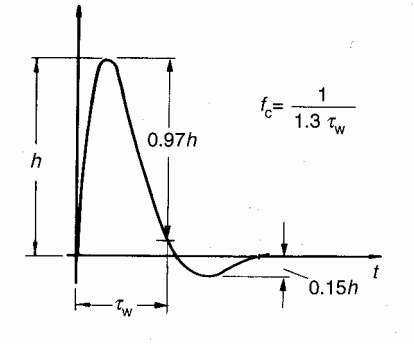

Figure 4.2.2 Optimum square-wave test response, **Bruun, 1995**

4.2.1 General hot wire equation

To examine the behaviour of the hot wire, the general hot wire equation must first be derived. This equation will be used to examine both the steady state response of the hot wire, discussed here, and its frequency response, discussed later. By considering a small circular element of the hot wire, Figure 4.2.3, an energy balance can be performed, assuming a uniform temperature over its cross-section:

$$I^2 \delta R_w = \rho_w c_w \frac{\partial T_w}{\partial t} A \delta x + k_w A \frac{\partial T_w}{\partial x} + h \pi d \left(T_w - \eta T_o\right) \delta x - k_w A \left(\frac{\partial T_w}{\partial x} + \frac{\partial^2 T_w}{\partial x^2} \delta x \right) + \sigma \varepsilon \left(T_w^4 - T_{sur}^4\right) \pi d \delta x \quad \textbf{4.2.1}$$

This can be simplified, **Højstrup et al., 1976**, to give the general hot wire equation:

$$K_1 \frac{\partial T_w}{\partial t} = \frac{\partial^2 T_w}{\partial x^2} - \beta_1 T_w + K_2 T_a - K_3 , \qquad \textbf{4.2.2}$$

if radiation is neglected. The constants are given by:

$$K_1 = \frac{\rho_w c_w}{k_w}, \qquad \textbf{4.2.3}$$

$$\beta_1 = \frac{h\pi d}{k_w A} - \frac{\alpha I^2 \rho_{ref}}{k_w A^2}, \qquad \textbf{4.2.4}$$

$$K_2 = \frac{h\pi d}{k_w A}, \qquad \textbf{4.2.5}$$

$$K_3 = \frac{I^2 \rho_{ref}}{k_w A^2}\left(\alpha T_{ref} - 1\right). \qquad \textbf{4.2.6}$$

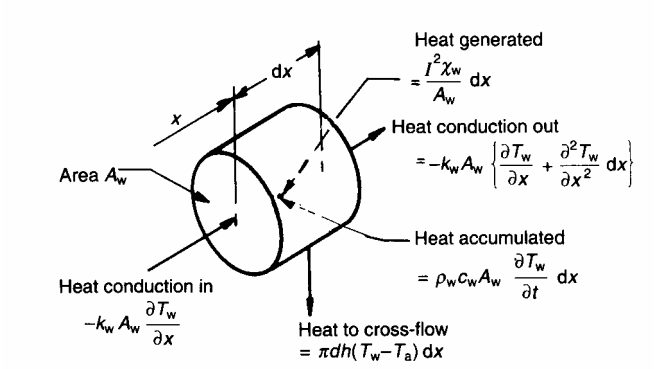

Figure 4.2.3 Heat balance for an incremental element, **Bruun, 1995**

The two main assumptions made in deriving equation 4.2.2 are that the radial variations in wire temperature and the radiation heat transfer are negligible: both of these will be justified briefly. The radiation term in equation 4.2.1 can be compared with any other term to assess its relative importance: the term chosen here is the fourth term in equation 4.2.1, giving a ratio:

$$Ratio = \frac{\sigma \varepsilon}{h T_a}\left(T_w^4 - T_a^4\right). \qquad \textbf{4.2.7}$$

Typical flow conditions over a typical hot wire give a ratio of 0.048 %.

The effects of radial variations are slightly more complex, but a simple case can be developed whereby the temperature is assumed to vary only in the radial direction. Performing a heat balance on the wire gives:

$$-\frac{I^2 \rho_w}{k_w A^2} = \frac{1}{r}\frac{\partial}{\partial r}\left(r \frac{\partial T}{\partial r}\right). \qquad \textbf{4.2.8}$$

If the change in resistivity with temperature is neglected, this yields the solution:

$$T_w(r) = const - \frac{I^2 \rho_w}{k_w A^2} \frac{r^2}{4}, \qquad \textbf{4.2.9}$$

where the constant is found from an energy balance at the surface. The maximum change across the wire as a ratio of the difference in temperature driving the heat transfer is then:

$$Ratio = \frac{1}{4} \frac{k}{k_w} Nu. \qquad \textbf{4.2.10}$$

For typical conditions at stage exit, the ratio is 0.022 %. Since these two effects are clearly negligible, equation 4.2.2 can be used as the general hot wire equation.

4.2.2 Steady state solution

The general steady state solution to Equation 4.2.2, assuming that $\overline{\beta}_1 > 0$, is found by applying the boundary condition and defining the mean wire temperature:

$$\overline{T}_w = \overline{T}_a \quad \text{at} \quad x = \pm l, \qquad \textbf{4.2.11}$$

$$T_m = \frac{1}{2l} \int_{-l}^{+l} \overline{T}_w dx. \qquad \textbf{4.2.12}$$

The non-dimensional steady state wire temperature distribution is then:

$$\frac{\overline{T}_w - \overline{T}_a}{T_m - \overline{T}_a} = \frac{\left[1 - \frac{\cosh\left(\sqrt{\overline{\beta}_1} x\right)}{\cosh\left(\sqrt{\overline{\beta}_1} l\right)}\right]}{\left[1 - \frac{1}{\left(\sqrt{\overline{\beta}_1} l\right)} \tanh\left(\sqrt{\overline{\beta}_1} l\right)\right]}, \qquad \textbf{4.2.13}$$

which is only a function of the Biot number, $\sqrt{\overline{\beta}_1} l$, Figure 4.2.4.

A heat balance can then be performed over the whole wire, assuming that the flow conditions are uniform over the wire:

$$\overline{I}^2 R_w = \overline{H}_{cond} + \overline{H}_{conv}. \qquad \textbf{4.2.14}$$

The two heat transfer components can be found from the flow conditions and the wire temperature distribution:

$$\overline{H}_{conv} = 2l\pi d\overline{h}\left(T_m - \overline{T}_a\right), \qquad \textbf{4.2.15}$$

$$\overline{H}_{cond} = 2k_w A \left|\frac{\partial \overline{T}_w}{\partial x}\right|_{x=l}, \qquad \textbf{4.2.16}$$

to give a steady state heat transfer equation:

$$\overline{I}^2 R_w = 2\pi \overline{h}_c dl\left(T_m - \overline{T}_a\right), \qquad \textbf{4.2.17}$$

where the corrected heat transfer coefficient is given by:

$$\bar{h}_c = \bar{h} + \frac{dk_w}{4l}\left(\frac{\sqrt{\bar{\beta}_1}\tanh\left(\sqrt{\bar{\beta}_1}l\right)}{1-\frac{\tanh\left(\sqrt{\bar{\beta}_1}l\right)}{\sqrt{\bar{\beta}_1}l}}\right). \qquad \textbf{4.2.18}$$

If the Biot number is larger than approximately 3, as is usually the case, in terms of Nusselt number this approximates to, **Bradshaw, 1971**:

$$Nu_c = Nu + \frac{1}{2}\frac{d}{l}\sqrt{\frac{k_w}{k}}\sqrt{Nu}\,, \qquad \textbf{4.2.19}$$

giving the steady state calibration equation:

$$\bar{E}_w^2 = 2\pi klR_w Nu_c\left(T_m - \bar{T}_a\right), \qquad \textbf{4.2.20}$$

where the wire resistance is set by adjusting the Wheatstone bridge and is related to the mean wire temperature by means of the temperature coefficient of resistance. To reduce the proportion of heat transfer by conduction for given flow conditions the wire length to diameter ratio must thus be increased. Although the conduction end effect can be compensated out using equation 4.2.19, this is normally done automatically in the calibration. Equation 4.2.20 shows that the variations in the wire voltage are only dependent upon fluctuations in the Nusselt number and the temperature difference between the hot wire and the flow: both of these will now be examined.

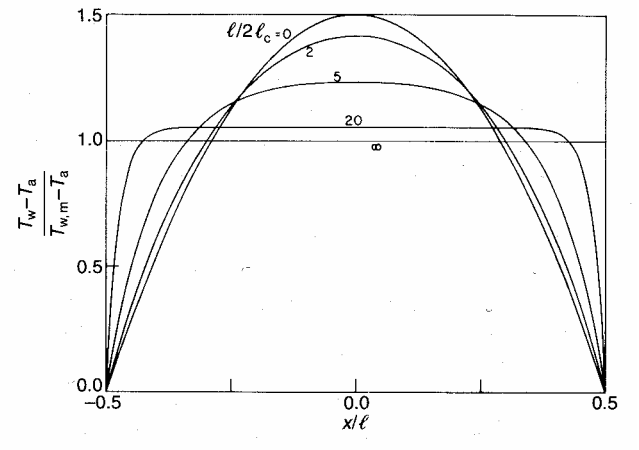

Figure 4.2.4 Steady state temperature distribution, **Freymuth, 1979**

4.2.3 Nusselt number dependence

Due to the general engineering importance of heat transfer from a heated cylinder, the dependence of the Nusselt number on the flow conditions has been the subject of much research. However, only results that are relevant to the flow field in which the measurements are to be made are given here. Since this flow field is at approximately Mach 0.45, the flow field is subsonic but compressible.

In compressible flow regimes there are a considerable number of dependent parameters, each of which must be examined. The most general relationship is, **Bruun, 1995**:

$$Nu = Nu\left(\mathrm{Re}, \mathrm{Pr}, Kn, M, \tau, l/d\right), \qquad \textbf{4.2.21}$$

where the temperature recovery factor, **Kovasznay, 1950**, is defined as:

$$\tau = \frac{T_w - \eta T_o}{T_o}, \qquad \textbf{4.2.22}$$

and the recovery factor, η, is defined as the ratio of the recovery temperature to the total temperature. The Knudsne number is defined as the ratio of the gas mean free path to the wire diameter. The influence of the length/diameter ratio is due to the conduction end effects. Equation 4.2.21 can be simplified, however, for a given wire at a given overheat ratio in a given fluid to:

$$Nu = Nu\left(\mathrm{Re}, M\right), \qquad \textbf{4.2.23}$$

since the Prandtl number is nearly constant for gases over a wide range of temperatures and pressures and the other parameters are set by the wire dimensions and temperature. The influence of the Knudsen number is neglected here since it is only significant in low-density flows.

The most exhaustive correlation of experimental results in the form of equation 4.2.23 has been performed by **Dewey, 1965**, in the ranges 0.02 < Re < 1000 and M > 0.2:

$$Nu_o\left(\mathrm{Re}_o, M\right) = Nu_o\left(\mathrm{Re}_o, \infty\right)\Phi\left(\mathrm{Re}_o, M\right); \qquad \textbf{4.2.24}$$

where:

$$Nu_o\left(\mathrm{Re}_o, \infty\right) = \mathrm{Re}_o^n\left[0.1400 + \left(\frac{0.2302\,\mathrm{Re}_o^{0.7114}}{15.44 + \mathrm{Re}_o^{0.7114}}\right) + \left(\frac{0.01569}{0.3077 + \mathrm{Re}_o^{0.7378}}\right)\left(\frac{15}{15 + \mathrm{Re}_o^3}\right)\right], \qquad \textbf{4.2.25}$$

$$n = 1 - \frac{1}{2}\left(\frac{\mathrm{Re}_o^{0.6713}}{2.571 + \mathrm{Re}_o^{0.6713}}\right), \qquad \textbf{4.2.26}$$

$$\Phi\left(\mathrm{Re}_o, M\right) = 1 + A(M)\left[1.834 - \left(\frac{1.634\,\mathrm{Re}_o^{1.109}}{2.765 + \mathrm{Re}_o^{1.109}}\right)\right]\left[1 + \left(0.300 - \frac{0.0650}{M^{1.670}}\right)\left(\frac{\mathrm{Re}_o}{4 + \mathrm{Re}_o}\right)\right], \qquad \textbf{4.2.27}$$

and:

$$A(M) = \frac{0.6039}{M} + 0.5701\left[\left(\frac{M^{1.222}}{1 + M^{1.222}}\right)^{1.569} - 1\right]. \qquad \textbf{4.2.28}$$

Although this correlation is complicated to use analytically, it can easily be stored numerically and is thus used in this form throughout this thesis.

4.2.4 Temperature dependence

The measured wire voltage is also dependent upon the temperature difference between the wire and the flow. Unless this temperature difference is measured or already known a measurement error will

result, although this error can be minimised for small temperature fluctuations by operating the wire at a high temperature and calibrating the wire at the mean flow temperature. A means of compensation will otherwise be required: there are two main practical ways, **Bruun, 1995**:

1. *Automatic compensation*: Use a temperature sensor in the Wheatstone bridge.
2. *Analytical correction*: Measure the flow temperature separately and compensate using the heat transfer equation.

Since automatic compensation has a bandwidth of approximately 100 Hz, analytical correction is the only means of compensation at most experimental frequencies.

4.3 Frequency response

The steady state solution has shown that there are two dominant heat transfer mechanisms, but that the steady state heat transfer by conduction is normally automatically compensated for in the calibration. However, if the two heat transfer mechanisms behave differently with frequency, a steady state calibration will become inaccurate at any frequency. The frequency response of a hot wire will thus be examined in detail, examining previous attempts before developing a complete theoretical solution.

4.3.1 Previous research

Højstrup et al., 1976, examined the effects of fluctuations in the flow temperature on the wire temperature distribution. However, no fluctuations in heat transfer coefficient or current were considered, and the overall wire resistance was not kept constant. **Freymuth, 1979**, defined a fluctuation ratio as the ratio of heat transfer at high frequencies, when the conduction fluctuations drop to zero, to that at steady state conditions. Although the mean wire temperature was kept constant, the results are only applicable for low overheat ratios and no general solution is given, although two distinct break frequencies were found. **Parantheon et al., 1983**, performed a more detailed analysis, which was confirmed well by experimental results up to the maximum experimental frequency of 800 Hz. In this case, as with **Freymuth, 1979**, the dependent parameters are not clearly expressed, nor is the physical background clear.

The most recent attempt to compensate for high frequency effects experimentally, **Brouckaert, 1998**, used a step change in flow temperature. A series of first order differential equations was developed and used to compensate for conduction effects at all frequencies. This has the advantages of being experimentally derived and applicable to any hot wire: however, neither the derivation nor the application of this procedure is described clearly. A complete theoretical analysis of the frequency response of a hot wire is thus performed here for the first time. This provides compensation factors for any hot wire at any frequency, clearly outlining the physical basis for the solution.

4.3.2 Complete theoretical solution

The complete solution requires the variation of all the parameters that depend upon the flow field: the current, heat transfer coefficient, flow temperature and wire temperature distribution. The general hot wire equation, equation 4.2.2, is separated into two equations, representing the steady state and the fluctuating components, assuming small fluctuations:

$$\frac{\partial^2 \overline{T}_w}{\partial x^2} - \overline{\beta}_1 \overline{T}_w = \overline{K}_3 - \overline{K}_2 \overline{T}_a \,, \qquad \textbf{4.3.1}$$

$$\overline{K}_1 \frac{\partial T_w'}{\partial t} = \frac{\partial T_w'}{\partial x^2} - \overline{\beta}_1 T_w' - \beta_1' \overline{T}_w + \overline{K}_2 T_a' + K_2' \overline{T}_a - K_3', \qquad \textbf{4.3.2}$$

where the steady state solution is given in equation 4.2.13. To solve equation 4.3.2 each component is assumed to vary sinusoidally:

$$T_w' = Z_w e^{jwt} \,, \qquad \textbf{4.3.3}$$

$$T_a' = Z_a e^{jwt} \,, \qquad \textbf{4.3.4}$$

$$h' = Z_h e^{jwt} \,, \qquad \textbf{4.3.5}$$

$$I' = Z_I e^{jwt} \,. \qquad \textbf{4.3.6}$$

Substitution of these into equation 4.3.2 gives:

$$Z_w \left[\overline{\beta}_1 + j\omega \overline{K}_1\right] - \frac{\partial Z_w^2}{\partial x^2} = \overline{K}_2 Z_a + \left[\overline{T}_a - \overline{T}_w\right] \frac{\pi d}{k_w A} Z_h + \left[\frac{2\alpha \bar{I} \rho_{ref}}{k_w A^2} \overline{T}_w - \frac{2\bar{I}\rho_{ref}}{k_w A^2}\left(\alpha T_{ref} - 1\right)\right] Z_I \,. \qquad \textbf{4.3.7}$$

This can then be solved in a similar way to the steady state solution, given that the steady state wire temperature distribution is dependent on *x*. If we collect terms on the right hand side as constants and functions of *x*, and define a new parameter, equation 4.3.7 reduces to:

$$\overline{\beta}_{11} Z_w - \frac{\partial^2 Z_w}{\partial x^2} = Y_1 + Y_2 \cosh\left(\sqrt{\overline{\beta}_1}\, x\right), \qquad \textbf{4.3.8}$$

where Y_1 and Y_2 are found from substituting equation 4.2.13 into equation 4.3.7 and:

$$\overline{\beta}_{11} = \overline{\beta}_1 + j\omega \overline{K}_1, \qquad \textbf{4.3.9}$$

The solution to equation 4.3.8 is of the form:

$$Z_w = C_1 + C_2 \cosh\left(\sqrt{\overline{\beta}_1}\, x\right) + C_3 \cosh\left(\sqrt{\overline{\beta}_{11}}\, x\right), \qquad \textbf{4.3.10}$$

where the constants can be found from substitution into equation 4.3.7 and by using the boundary condition and the general frequency response of the wire supports, $F(j\omega)$:

$$\int_{x=-l}^{x=l} Z_w dx = 0 \,, \qquad \textbf{4.3.11}$$

$$Z_w\left(x = \pm l\right) = F\left(j\omega\right) Z_a \,. \qquad \textbf{4.3.12}$$

The relationship between the variations in wire current, heat transfer coefficient and flow temperature can then be expressed in the form:

$$\frac{Z_I}{\bar{I}} = G_a \frac{Z_a}{\bar{T}_a} + G_h \frac{Z_h}{\bar{h}}. \qquad \textbf{4.3.13}$$

To simplify the solution, a non-dimensional frequency and two other parameters are used:

$$\omega' = j\omega \frac{\bar{K}_1}{\bar{\beta}_1}, \qquad \textbf{4.3.14}$$

$$\xi_1 = \sqrt{\bar{\beta}_1} l \coth\left(\sqrt{\bar{\beta}_1} l\right), \qquad \textbf{4.3.15}$$

$$\xi_{11} = \sqrt{\bar{\beta}_{11}} l \coth\left(\sqrt{\bar{\beta}_{11}} l\right). \qquad \textbf{4.3.16}$$

Three slightly different definitions of overheat ratio are also used, where the overheat ratio is a non-dimensional measure of the rise in temperature of the hot wire:

$$a_{ref} = \alpha\left(T_m - T_{ref}\right), \qquad \textbf{4.3.17}$$

$$a_a = \alpha\left(T_m - \bar{T}_a\right), \qquad \textbf{4.3.18}$$

$$\tau = \frac{\left(T_m - \bar{T}_a\right)}{\bar{T}_a}. \qquad \textbf{4.3.19}$$

Equation 4.3.7 can then be reduced to a non-dimensional form, after considerable algebra:

$$G_a(\omega') = -\frac{1}{2\tau} \frac{(\xi_1 - 1)^2 \omega' \left[F(1+\omega')(1 + a_{ref} - a_a) + \left(\frac{\xi_{11} - 1}{\xi_1 - 1} \right) \left((\xi_1 - 1)(1 + a_{ref} - a_a) + \xi_1 a_a \right) \right]}{\xi_1 \left[(1+\omega') a_a (\xi_1 - \xi_{11}) + \omega'(\xi_{11} - 1) \left[(\xi_1 - 1)(1 + a_{ref} - a_a) + \xi_1 a_a \right] \right]}, \qquad \textbf{4.3.20}$$

$$G_h(\omega') = \frac{1}{2} \frac{\left[(\xi_1 - 1)(1 + a_{ref} - a_a) + \xi_1 a_a \right] \left[(\xi_1 - \xi_{11}) + \omega' \xi_{11} (\xi - 1) \right]}{\xi_1 \left[(1+\omega') a_a (\xi_1 - \xi_{11}) + \omega'(\xi_{11} - 1) \left[(\xi_1 - 1)(1 + a_{ref} - a_a) + \xi_1 a_a \right] \right]}. \qquad \textbf{4.3.21}$$

Some simplifications can be made if it is again assumed that the Biot number is larger than approximately 3. ξ_1 can be found from the overheat ratio if the ratio of heat transfer by conduction to heat transfer by convection is known. This ratio is defined as:

$$\chi = \frac{d}{2l} \sqrt{\frac{k_w}{kNu}}, \qquad \textbf{4.3.22}$$

from equation 4.2.19. This yields a relationship:

$$\xi_1 = \frac{1}{\chi} \sqrt{\frac{(\xi_1 - 1)(1 + a_{ref} - a_a)}{(\xi_1 - 1)(1 + a_{ref} - a_a) + \xi_1 a_a}}, \qquad \textbf{4.3.23}$$

which allows ξ_1 to be found iteratively once the overheat and heat transfer ratios are known. Equation 4.3.16 can also be simplified for large Biot numbers to give:

$$\xi_{11} = \xi_1 \sqrt{1 + \omega'}. \qquad \textbf{4.3.24}$$

There are thus only six dependent parameters: three forms of the overheat ratio (τ, a_{ref}, a_a), the frequency response of the supports ($F(j\omega)$), the ratio of heat transfer terms (χ) and the non-dimensional frequency (ω'). The parameter used to non-dimensionalise the frequency represents the attenuation frequency of the heat waves along the wire, and can be thought of as the time constant of the wire, M_w:

$$M_w = \frac{\overline{K}_1}{\overline{\beta}_1} = \frac{\rho_w c_w l^2}{k_w \xi_1^2}. \qquad \textbf{4.3.25}$$

The advantage of Constant Temperature Anemometry is shown here in the reduction of the time constant and the resulting increase in the bandwidth of the hot wire by a factor ξ_1^2 from the value without feedback. This time constant is also given in **Freymuth, 1979**, but without the factor ξ_1^2: an extra factor is used to approximate for this effect, given as approximately 0.1 for the attenuation frequency. This is an encouraging agreement with equation 4.3.25 since the factor ξ_1^2 is generally large. The only parameter that needs further investigation before examining the solutions to equations 4.3.20 and 4.3.21 is the frequency response of the wire supports.

4.3.3 Frequency response of wire supports

The earliest model, **Højstrup et al., 1976**, was a simple first-order low-pass filter.

$$\frac{Z_w(x = \pm l)}{Z_a} = \frac{1}{1 + j\omega M_s}. \qquad \textbf{4.3.26}$$

A similar model was used by **Freymuth, 1979**, treating the supports as solid bodies of uniform temperature to give a first order differential equation with time constant:

$$M_s = \frac{\rho_s V_s c_s}{h A_s}, \qquad \textbf{4.3.27}$$

where V_s and A_s are the volume and surface area of the support. The same result is quoted by **Parantheon et al., 1983**. Although there is general agreement on the form of equation 4.3.26, there is little information on the calculation of the time constant, as even equation 4.3.27 is difficult to use in practice, although a value of 1 second seems to be the most common value. This value has thus been adopted throughout this analysis: its precise value is relatively unimportant, since the corresponding break frequency is much lower than most experimental measurements.

4.3.4 Steady state response

Before examining the general frequency response of the hot wire, the steady state response is derived, since this determines the reference behaviour with which the general frequency response must be compared and it can also be compared with experimental calibration results. By letting the frequency

tend to zero in equations 4.3.20 and 4.3.21, the steady state values can be found for large Biot numbers:

$$(G_a)_{ss} = -\frac{(\xi_1 - 1)^2}{\tau} \frac{(1 + a_{ref})}{\left[2(\xi_1 - 1)^2 (1 + a_{ref} - a_a) + \xi_1 a_a (2\xi_1 - 3)\right]}, \qquad \textbf{4.3.28}$$

$$(G_h)_{ss} = \frac{((\xi_1 - 1)(1 + a_{ref} - a_a) + \xi_1 a_a)(2\xi_1 - 3)}{2\left[2(\xi_1 - 1)^2 (1 + a_{ref} - a_a) + \xi_1 a_a (2\xi_1 - 3)\right]}. \qquad \textbf{4.3.29}$$

These can be compared with the ideal behaviour, i.e. for no conduction or an infinitely long wire, by allowing χ to tend to zero, and hence ξ_1 to tend to infinity:

$$(G_a)_{ss,ideal} = -\frac{1}{2\tau}, \qquad \textbf{4.3.30}$$

$$(G_h)_{ss,ideal} = \frac{1}{2}. \qquad \textbf{4.3.31}$$

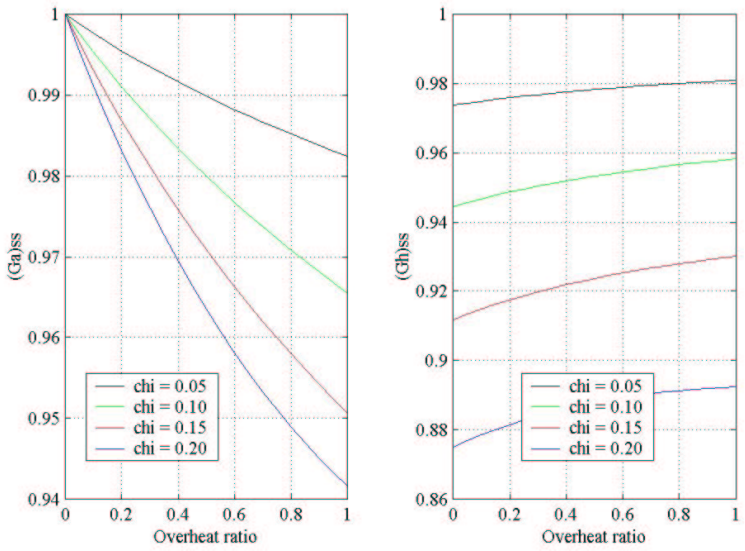

Figure 4.3.1 Variation in sensitivity coefficients with overheat ratio (*a*) and heat transfer ratio (χ, *chi*)

The ratio of the actual values to the ideal values gives a measure of the errors introduced by the conduction effects. To simplify the equations slightly, it is assumed that the reference and mean flow temperatures are the same:

$$\frac{(G_a)_{ss}}{(G_a)_{ss,ideal}} = \frac{2(\xi_1 - 1)^2 (1 + a)}{\left[2(\xi_1 - 1)^2 + \xi_1 a (2\xi_1 - 3)\right]}, \qquad \textbf{4.3.32}$$

$$\frac{(G_h)_{ss}}{(G_h)_{ss,ideal}} = \frac{((\xi_1 - 1) + \xi_1 a)(2\xi_1 - 3)}{\left[2(\xi_1 - 1)^2 + \xi_1 a (2\xi_1 - 3)\right]}. \qquad \textbf{4.3.33}$$

Since ξ_1 can be found using the overheat and heat transfer ratios from equation 4.3.23, equations 4.3.32 and 4.3.33 can be plotted against these ratios, Figure 4.3.1. Although the temperature

sensitivity is roughly proportional to both ratios, the heat transfer coefficient sensitivity is largely independent of the overheat ratio. There is a significant effect on both if the heat transfer ratio is large.

4.3.5 General frequency response

Since the steady state heat transfer by conduction is automatically compensated for in the calibration, only the divergence of the hot wire from the steady state behaviour is of interest. Equations 4.3.20 and 4.3.21 can thus be plotted as ratios of the steady state solution in equations 4.3.28 and 4.3.29 against frequency for typical flow conditions and varying overheat ratio, Figure 4.3.2. This is because the flow field in which measurements are to be taken is fixed and it is only the properties and overheat of the wire that can be chosen. The flow parameters used here are a total pressure of 3.25 bar, total temperature of 297 K, Mach number of 0.45 and wire diameter and length of 5 μm and 1.2 mm. Unless otherwise stated, these values are used throughout.

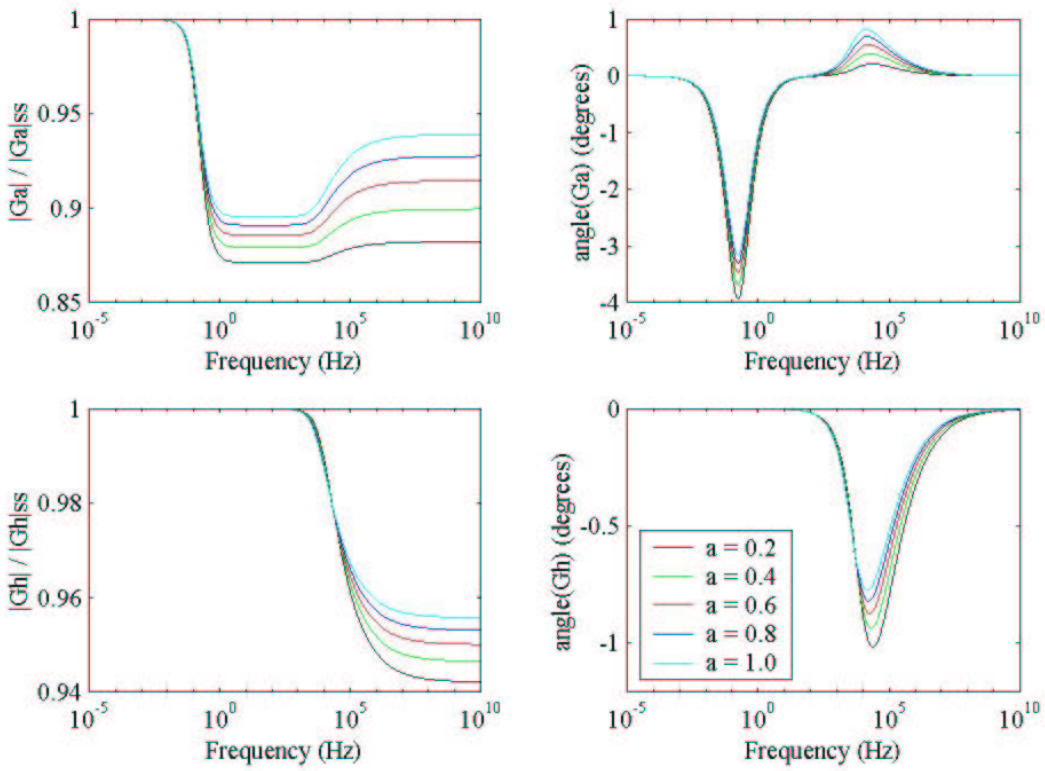

Figure 4.3.2 Variation of sensitivity coefficients with frequency (*f*) and overheat ratio (*a*)

There are two break frequencies, one due to the attenuation of heat transfer to the supports, and the other due to the attenuation of heat waves along the wire. The first only affects the sensitivity to temperature fluctuations and occurs at approximately 1 Hz, but the second affects both sensitivities. Although it starts to occur at approximately 10 kHz, its effects last until approximately 1MHz. The phase errors are negligible.

Since most experimental frequencies lie between the two break frequencies, the plateau level in this region is of greatest interest. Although the heat transfer sensitivity coefficient remains unchanged, the temperature sensitivity coefficient can be found by setting $F(j\omega)$ to zero but assuming that $\omega' << 1$:

$$\frac{(G_a)_{mf}}{(G_a)_{ss}} = \frac{\left((\xi_1 - 1)(1 + a_{ref} - a_a) + \xi_1 a_a\right)}{\xi_1 (1 + a_{ref})}, \qquad \textbf{4.3.34}$$

which can be simplified if the reference and mean flow temperatures are equal:

$$\frac{(G_a)_{mf}}{(G_a)_{ss}} = \frac{(\xi_1 (1 + a) - 1)}{\xi_1 (1 + a)}. \qquad \textbf{4.3.35}$$

This is almost independent of the overheat ratio, Figure 4.3.3, and the difference between this value and the ideal value is approximately equal to the heat transfer ratio, χ. For given flow conditions this difference can only be reduced by an increase in the length/diameter ratio. Since this reduces the spatial resolution, some compromise is inevitable.

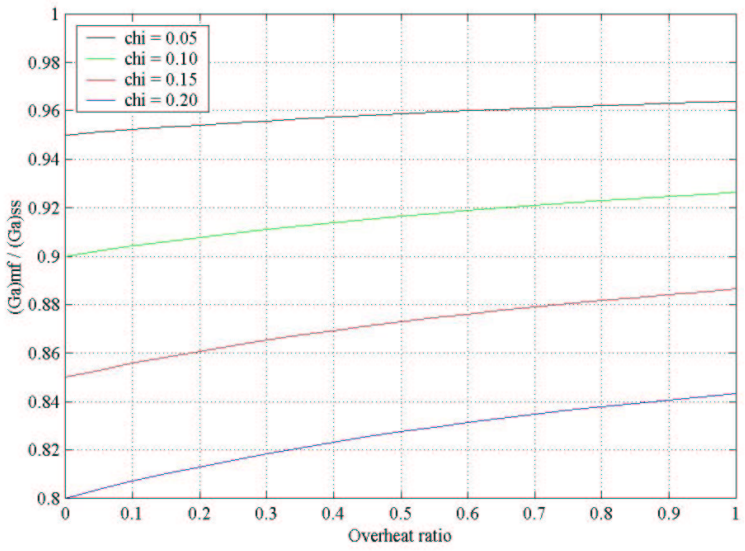

Figure 4.3.3 Variation in temperature sensitivity between the two break frequencies with overheat ratio (a) and heat transfer ratio (χ, *chi*)

4.3.6 Summary

A complete theoretical analysis of the frequency response of a hot wire has been developed here for the first time. This has shown that a correction is needed for experimental results at any frequency above approximately 1 Hz, without which significant errors will result. This correction is due to the presence of heat transfer by conduction. Above this frequency up to approximately 10 kHz, the sensitivity to heat transfer coefficient remains unchanged but the sensitivity to temperature drops to a constant value with negligible phase shift. A compensation factor has thus been derived for any hot

wire that is solely dependent upon the overheat and heat transfer ratios. This will be examined further in Chapter 5, when other high frequency effects are considered and experimental validations are used.

4.4 Calibration

The general behaviour of hot wire anemometry has been examined in some detail, particularly the frequency response. The specific hot wire probes used in this thesis are now also examined in detail, particularly their calibrations. This enables the measurement capabilities of these hot wire probes to be determined, their measurement accuracy assessed and the steady state sensitivities to be determined. Since the heat transfer from a hot wire is dependent upon the flow yaw and pitch angles, as well as the Reynolds number, the Mach number and the total temperature, the hot wire probes must be calibrated over all five flow parameters.

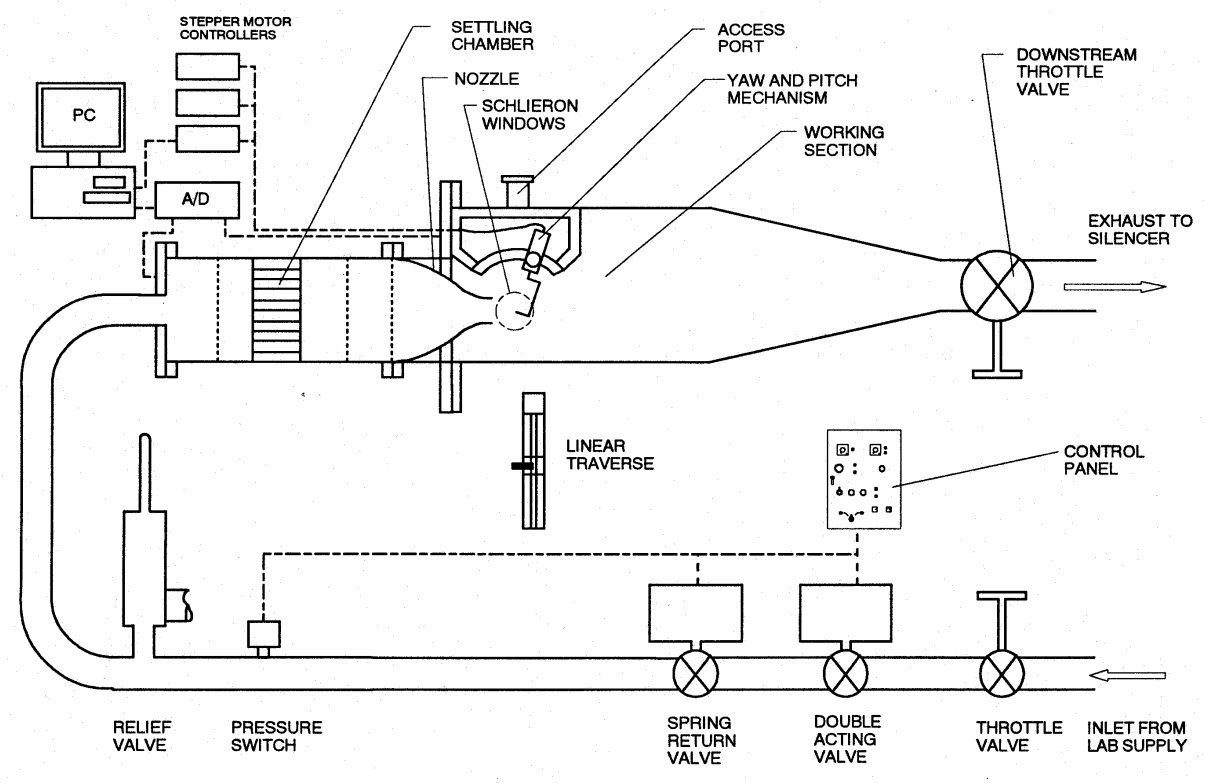

Figure 4.4.1 Schematic of calibration wind tunnel, **Slater, 1993**

All the hot wire probes are calibrated in the dedicated calibration facility, Figure 4.4.1, **Slater, 1993**. By means of two throttle valves, upstream and downstream of the nozzle, the Reynolds and Mach numbers can be set independently before the hot wire probe is traversed over a range of flow angles by a special yaw and pitch mechanism. The facility is then operated at as many different conditions as required. The only dependent flow parameter that cannot be set independently is the total temperature: however, this can be compensated for using equation 4.2.20.

Three different double hot wire probes have been calibrated here. They are all standard commercial probes, Figure 4.4.2, although the wire diameter has been increased from 5 μm to 9 μm to increase the wire strength. The increase in strength was found to be necessary as the original 5 μm diameter wire was insufficiently strong to withstand the highly loaded and highly unsteady flow field in the ORF. The original welding technique used was also found to be too weak. The wires were thus welded and soldered to the prongs: together with the increase in wire diameter, this enabled the wires to last almost indefinitely in the ORF. The strength was largely dependent upon the quality of the soldering and considerable practice was required to achieve suitably strong joints. The prong surface had to be thoroughly cleaned, removing any previous traces of solder, before welding could be performed successfully. A reasonably large amount of solder was then required to cover the end of the wire completely. The wires then tended to fail either immediately or to last almost indefinitely, allowing the strength of the joint in the ORF to be assessed rapidly.

The details of the probes and their calibrations are given in Table 4.4.1. Probes B and C are relatively insensitive to pitch angle, since the mean flow pitch angle is approximately zero, in agreement with **Slater, 1993**. Probe A, however, is sensitive to both pitch and yaw angle. Probes A and B were calibrated twice to assess the calibration drift errors, whilst probe C was re-calibrated following the breakage of the first set of hot wires.

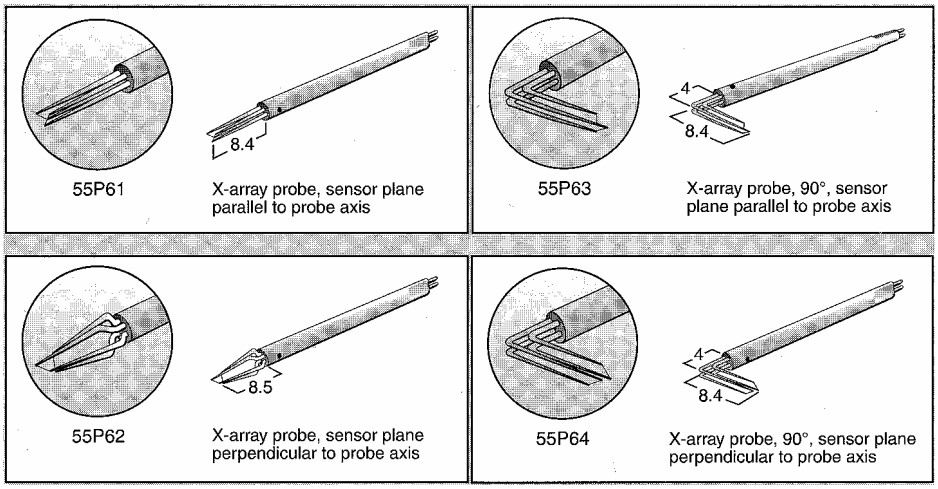

Figure 4.4.2 Hot wire probes, **Dantec, 1996**

Probe	Probe name	Calibration 1	Calibration 2
A	55P61	410	420
B	55P62	400	430
C	55P64	270	280

Table 4.4.1 Calibration details

Since many calibration equations have been proposed for the various flow parameters, especially for variations in flow angle, it was decided to examine the dependence on each of these separately. Similarly to **Slater, 1993**, the wire temperatures were set at 500 K to optimise the frequency response and temperature sensitivity. Since the hot wires are at 90° to each other, yaw angle fluctuations of approximately ± 45° can be resolved: hence a range of ± 54° was chosen to cover the complete yaw angle range. A range of pitch angle of -24.4° to +30.6° was chosen: this was asymmetrical due to the non-zero expected mean pitch angle in the ORF.

The Dewey correlation, equations 4.2.24 to 4.2.28, was used to convert the Reynolds and Mach numbers to a Nusselt number, which was then used in the general calibration equation, equation 4.2.20, in the form:

$$E^2 = \left(ANu + B\sqrt{Nu}\right)\left(T_m - \eta T_o\right). \qquad \textbf{4.4.1}$$

A best fit was found for the calibration coefficients *A* and *B* for every combination of yaw and pitch angle. Since the calibration fit is reduced to one variable, the Nusselt number, only a relatively small number of operating conditions were required to obtain the values of *A* and *B*. Equation 4.4.1 gave a consistent variation in *A* and *B* over yaw and pitch angle and encouragingly low errors over the entire calibration, Table 4.4.2. Although different forms of equation 4.4.1 could be found that reduced the rms error slightly, the calibration coefficients were much more random, giving a much less physically reasonable solution.

Probe calibration	Hot wire 1 rms voltage error	Hot wire 2 rms voltage error
C (270)	0.254 %	0.226 %
C (280)	0.218 %	0.227 %
B (400)	0.355 %	0.264 %
A (410)	0.276 %	0.328 %
A (420)	0.248 %	0.493 %
B (430)	0.526 %	0.385 %

Table 4.4.2 Percentage rms voltage errors for each calibration

However, since only a relatively poor fit was found to any form of angle correlation, probably due to the very wide range of flow angle, the calibration was stored as a set of values for *A* and *B* for each combination of yaw and pitch angle. Although this gives the greatest accuracy, it is somewhat complicated, since the complete heat transfer relationship involves the use of equation 4.4.1 together with a lookup table for yaw and pitch angle.

To quantify the errors involved in fitting the data to the calibration equation for Nusselt number, the measured voltages can be used in the calibration to solve for Nusselt number and yaw angle, assuming that the pitch angle is correct. The rms errors give a measure of the accuracy of using the calibration equation in terms of flow properties. The valid measurement range of yaw angle for each probe can also be found, since the calibrations turn back on themselves at extreme yaw angles.

The predicted and measured values of yaw angle are shown in Figures 4.4.3 and the rms errors in both yaw angle and Nusselt number against yaw angle in Figure 4.4.4, both for calibration 400. The agreement is very good for yaw angle apart from the two highest values of yaw angle, where the calibration turns back on itself. The valid angle range for this calibration is thus -43.2° to +21.6°. In this range the average errors in yaw angle and Nusselt number, using every data point, are very low. The calibrations are not quite symmetrical, since the probes are not exactly symmetrical and the prongs for one wire affect the flow field of the other. This effect also varies with the pitch angle, resulting in non-symmetrical calibrations, which must have their angle ranges examined carefully.

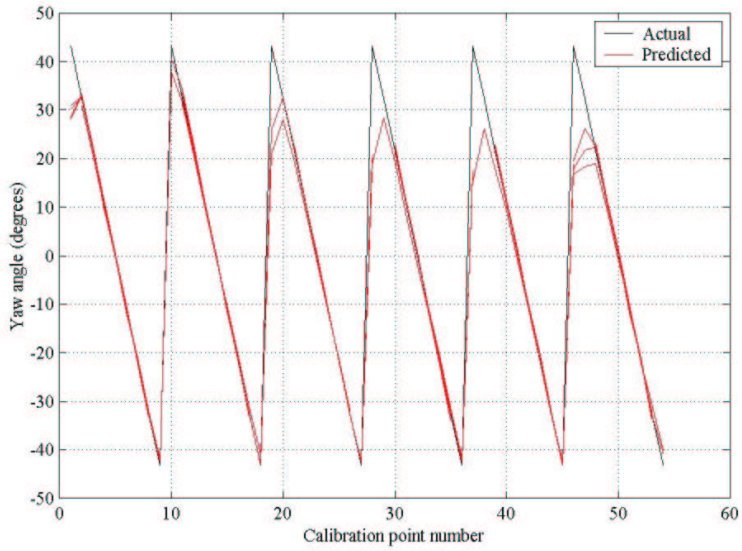

Figure 4.4.3 Comparison of predicted yaw angle against actual yaw angle, calibration 400

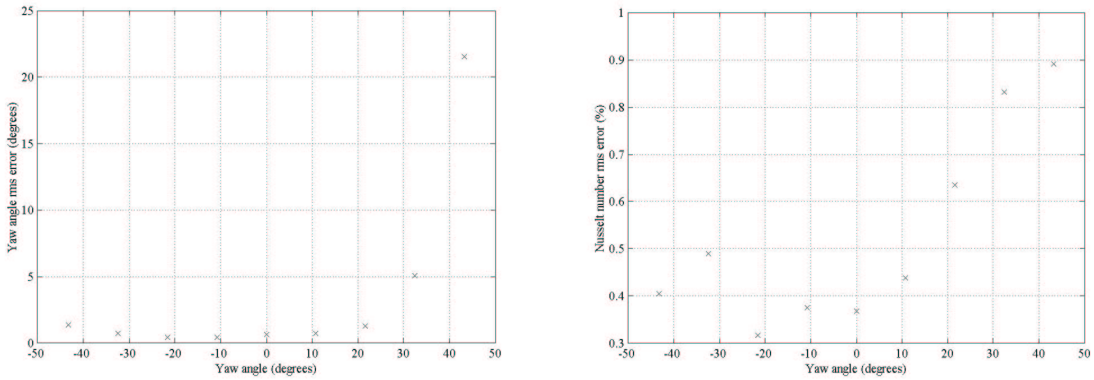

Figure 4.4.4 rms errors in yaw angle and Nusselt number, against yaw angle, calibration 400

Probe	Calibration	Useful yaw angle range		Yaw angle rms error	Nusselt number rms error
		Minimum	Maximum		
C	270	-28.8°	28.8°	0.98°	0.73 %
C	280	-36.0°	28.8°	0.70°	0.42 %
B	400	-43.2°	21.6°	0.79°	0.43 %
B	430	-32.4°	32.4°	1.45°	0.61 %
A	410	-43.2°	-10.8°	1.07°	0.61 %
A	420	-32.4°	-10.8°	4.19°	1.64 %

Table 4.4.3 Ranges and errors of hot wire calibrations

The same analysis has been performed for all the calibrations for probes B and C, with a similar approach for probe A, but solving for the pitch angle whilst keeping the yaw angle constant, Figure 4.4.5. The fit is particularly good towards the right hand side, where the yaw angle is large and negative. Although there are other values of yaw angle where the errors are small, these are harder to identify. The valid ranges of yaw angle and the rms errors are given in Table 4.4.3. For all the hot wire probes, the calibration errors are encouragingly small over large ranges of yaw angle. This gives a high level of confidence in the accuracy of any results obtained using these probes.

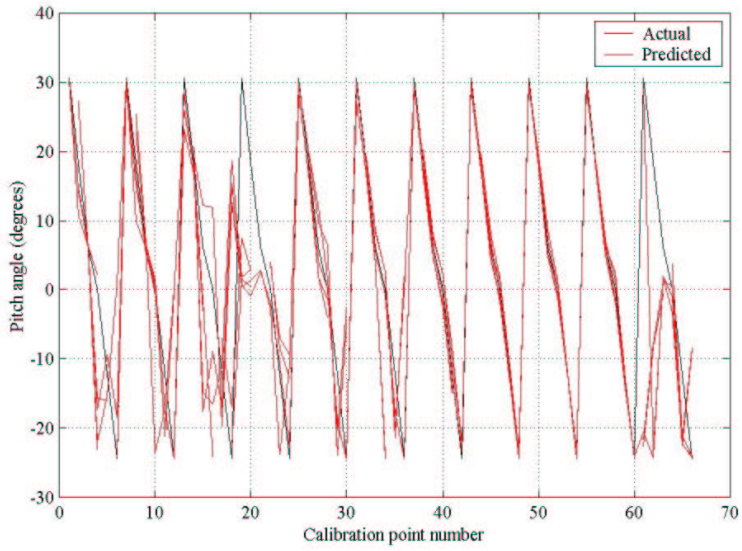

Figure 4.4.5 Comparison of predicted pitch angle against actual pitch angle, calibration 410

Since the hot wire probes were not calibrated immediately before use, the drift in the calibrations must also be checked. This was done for probe B by inserting the voltages calculated using the first calibration (400) into the second calibration (430). The wire temperatures were found to have dropped

slightly: since the probe had been used in the ORF six times between the two calibrations, this was probably due to slight oil burn on the hot wires. Once this had been compensated for and the small yaw angle offset removed, the errors over the intersection of the two useful calibration ranges were small: 1.72° in yaw angle and 1.47 % in Nusselt number.

Thus far all the calibrations are completely general and can be used to measure any combination of Reynolds number, Mach number, total temperature and flow angle with a high degree of accuracy. However, unless five hot wires are used, not all of these can be measured and some simplifications must be made. The usual assumption is that the effects of Mach number and total temperature are negligible in comparison with those of Reynolds number and flow angle, for example **Slater, 1993**. The accuracy of this assumption can be examined by means of a small-signal perturbation analysis.

For a given yaw and pitch angle, equation 4.4.1 gives:

$$\frac{E'}{\overline{E}} = S_{Nu}\frac{Nu'}{\overline{Nu}} + S_{To}\frac{T_o'}{\overline{T_o}}, \qquad \textbf{4.4.2}$$

where:

$$S_{Nu} = \frac{2A\overline{Nu} + B\sqrt{\overline{Nu}}}{4\left(A\overline{Nu} + B\sqrt{\overline{Nu}}\right)}, \qquad \textbf{4.4.3}$$

$$S_{To} = -\frac{1}{2\tau}. \qquad \textbf{4.4.4}$$

Some sensitivities, such as the sensitivity of Nusselt number to overheat ratio and the sensitivity of the recovery factor to Reynolds number and Mach number have been neglected, since these were all shown to be negligible, **Sheldrake, 1995**.

The Dewey correlation is then used to relate fluctuations in Nusselt number to fluctuations in Reynolds number and Mach number to give a relationship between voltage fluctuations and Reynolds number, Mach number and total temperature fluctuations:

$$\frac{E'}{\overline{E}} = S_{\mathrm{Re}}\frac{\mathrm{Re}'}{\overline{\mathrm{Re}}} + S_M\frac{M'}{\overline{M}} + S_{To}\frac{T_o'}{\overline{T_o}}. \qquad \textbf{4.4.5}$$

The typical flow conditions can be used to calculate typical sensitivity coefficients for probes similar to those in Figure 4.4.2 where *B/A* is found from equation 4.2.19:

$$\frac{E'}{\overline{E}} = 0.232\frac{\mathrm{Re}'}{\overline{\mathrm{Re}}} - 0.0775\frac{M'}{\overline{M}} - 0.666\frac{T_o'}{\overline{T_o}}. \qquad \textbf{4.4.6}$$

Although the sensitivity to Mach number is much less than the sensitivity to Reynolds number, as expected, it is not negligible. There is also a large sensitivity to total temperature, even at this high

overheat ratio, which has previously been ignored. If the Mach number is replaced by total pressure, to examine the effects of constant total properties, different sensitivity coefficients are found:

$$\frac{E'}{\overline{E}} = 0.131\frac{\mathrm{Re}'}{\overline{\mathrm{Re}}} + 0.101\frac{p_o'}{\overline{p_o}} - 0.717\frac{T_o'}{\overline{T_o}}. \qquad \textbf{4.4.7}$$

Different assumptions about the flow field thus give very different sensitivity coefficients and large errors will result from ignoring non-negligible fluctuations in flow parameters, even though the sensitivity to total temperature fluctuations is reduced at high frequencies.

Without a detailed knowledge of the flow field, it is difficult to calculate the errors due to different assumptions. However, to estimate the difference in Reynolds number when different assumptions are made, one experimental measurement made in the ORF was solved for Reynolds number using two sets of assumptions. The first was constant Mach number and total temperature and the second was constant total pressure and total temperature. There was zero difference in yaw angle, since the Nusselt number conversion is independent of yaw angle and constant total temperature was assumed for both solutions. However, the Reynolds number fluctuations were smaller for the first solution than for the second, as expected from equations 4.4.6 and 4.4.7. The difference was within approximately ± 7 %. Although the assumption of constant total pressure and total temperature seems more physically reasonable, and is used here, there will be quite a large unknown error in the measured Reynolds number due to assumptions about the flow field. Further work could usefully be carried out to improve this measurement accuracy, perhaps optimising the assumptions for different flow fields.

4.5 Measurement accuracy

To estimate the overall measurement accuracy of the hot wire probes used here, all the different sources of error must be considered. These are:

1. *Calibration measurement errors*: Errors in measuring the calibration flow parameters and hot wire voltages.
2. *Calibration equation errors*: Errors due to the fitting of a calibration equation, as well as solution of the calibration equation and lookup table.
3. *Calibration drift errors*: Errors caused by variations in calibration over time and over switching on and off of the feedback circuitry, as well as by probe contamination.
4. *Approximation errors*: Errors caused by assumptions about the flow field that are used to solve the calibration equations.
5. *High frequency errors*: Errors caused by the change in hot wire behaviour at high frequency.
6. *Spatial resolution errors*: Errors caused by spatial averaging of the flow field.
7. *Disturbance errors*: Errors caused by the probe interfering with the flow field.

The calibration measurement errors are found from a combination of the various sources of error. The error due to analogue to digital conversion is 60 μV, which is negligible in comparison with the noise on the data acquisition channels, and the error in probe angle is ± 0.1°, **Slater, 1993**. Since the static pressure transducer calibration drifts over time, five consecutive calibrations were performed, giving a rms error of 0.0624 %. The total temperature rms error is 0.0726 % from Chapter 3, giving errors in Reynolds and Mach numbers of 2.19 % and 2.81 % respectively for a mean Mach number of 0.45. The relatively large errors in Reynolds and Mach numbers are due to the small difference between the total and static pressure. The Dewey sensitivity coefficients then give a rms error in Nusselt number of approximately 2.2 %.

The calibration equation errors have already been quantified and are approximately 1° in yaw angle and 0.6 % in Nusselt number. The Nusselt number gives errors in either Reynolds number of 1.2 % or Mach number of 3.6 %. For the purposes of this analysis, the errors in Nusselt number are split half into Reynolds number and half into Mach number. The rms errors due to calibration drift have also already been calculated as 1.7° in yaw angle and 1.5 % in Nusselt number.

The largest source of error is the use of approximations in the assumptions about the flow field that are required to give a solution. Since the flow parameters are unknown, this error cannot be quantified accurately, although a typical value of 7 % error in Reynolds number was found earlier. The errors in flow angle measurement are small if all the hot wires are operated at very similar overheat ratios, since all the wire voltages are affected in the same way. These errors are reduced by the high frequency effects outlined earlier.

One of the main advantages of a hot wire probe is its excellent spatial resolution in comparison with other measurement techniques. However, if the flow field across the probe is not completely uniform, as is likely to be the case, there will be errors due to the difference in flow properties across the length of the hot wires and between the two hot wires. Results for a single hot wire showed that a reduction in the length to diameter ratio reduced this error, **Bruun, 1995**. Although the spatial resolution error cannot be calculated, comparison of the hot wire probe and flow field considered here with existing results shows that the errors are likely to be very small. The length of the wire should also be small in comparison with the wavelength of the flow phenomena passing along it: for hot wires placed perpendicular to the rotor blade trailing edge, the length of the wire should thus be smaller than approximately 25 mm. This is easily satisfied for the hot wire probes used here. The effects of probe disturbance are also unknown and will depend heavily on the given flow field in which the probe is placed. Again, one of the advantages of hot wire anemometry is that the small size of the probe reduces the probe blockage in comparison with similar measurement techniques.

Error source	Nusselt number % rms error	Reynolds number % rms error	Mach number % rms error	Flow angle rms error
Calibration measurement errors	2.2 %	2.2 %	2.8 %	0.1 °
Calibration equation errors	0.6 %	0.6 %	1.8 %	1.0 °
Calibration drift errors	1.5 %	1.5 %	4.2 %	1.7 °
Approximation errors	Unknown	Unknown	Unknown	Small
Spatial resolution errors	Small	Small	Small	Small
Disturbance errors	Small	Small	Small	Small
Total error	**2.7 %**	**2.7 %**	**5.4 %**	**2.0 °**

Table 4.5.1 Typical measurement errors for a single crossed hot wire at rotor exit

These measurement errors are summarised in Table 4.5.1, where the total rms errors are calculated from the sum of the variances. Since the approximation errors are likely to be large only for Reynolds and Mach numbers, the error in flow angle is shown here to be small. The other sources of error for Reynolds and Mach numbers are also small, showing that hot wire anemometry is a highly accurate and reliable technique, its accuracy only compromised by assumptions about the flow field.

To keep the measurement accuracy as high as possible, it is also important that as little error as possible is introduced by the analysis techniques used. Since these are presented in considerable detail elsewhere, **Miller, 1998**, only a brief summary is presented here, mainly describing the particular techniques used to obtain the experimental results presented in Chapters 6-8.

To prevent any distortion of the signal due to differences in the bandwidth of different hot wires, the wire voltages must be filtered down to the same bandwidth. By autocorrelating each rotor passing with the average, a phase shift can be found and removed from the voltage signals relative to the operating point time: the same phase shift is used for all the voltages to prevent any signal distortion. This phase shift arises from the rotor acceleration and the oscillation of the flow field. The small oscillations in the flow field must also be removed, using a low pass filter. Each recorded point is then converted to the relevant flow parameters over one complete revolution of the rotor disc either side of the operating point time to remove the effects of individual blades. Each point is converted individually since the calibrations are non-linear and a large error would result if the following analysis was performed on the voltage signals rather than on the flow parameters.

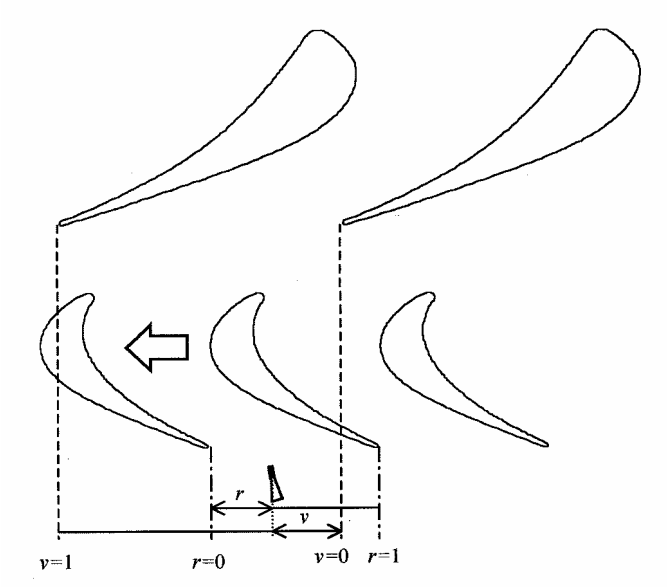

Figure 4.5.1 Vane and rotor co-ordinate systems, **Miller, 1998**

If the probe has remained stationary, the flow parameters can simply be ensemble averaged, thus requiring little filtering. If the probe has been traversed across the two vanes the position of the probe is calculated relative to both the upstream vanes and the rotor blades. The co-ordinate system used is the same as that from **Miller, 1998**, Figure 4.5.1, where the *v* and *r* co-ordinates are both measured from the relevant pressure surface to suction surface. The movement of the probe must be compensated for: the procedure is detailed in **Miller, 1998**, where the difference between the probe relative and the absolute Mach numbers is shown to be small.

The flow parameters can then be interpolated onto regular points in both vane and rotor co-ordinates. This must be done carefully, to preserve the bandwidth of the signal, and a cubic spline interpolation is thus used. Since the flow in the ORF is highly unsteady, considerable filtering is required to reduce the signals to their basic structure, as detailed in **Miller, 1998**. This gives a single 100-by-100 phase-phase matrix for each flow parameter in vane and rotor co-ordinates: this forms the basis for the vane-rotor interaction diagrams used later. The complete flow field is found by traversing the probe at a series of radial heights from hub to tip.

4.6 Summary and conclusions

Hot wire anemometry has been comprehensively reviewed in this Chapter as it provides the underlying technique behind all of the experimental measurements presented in this Thesis. Details have been given of the calibrations of the relevant hot wire probes, together with the first complete theoretical analysis of the frequency response of a hot wire. These have enabled the measurement accuracy to be experimentally determined and a completely general compensation factor to be developed to compensate experimental results for variations in hot wire behaviour at any frequency.

Calibration of these probes has enabled the dependence on Reynolds number, Mach number, total temperature, yaw angle and pitch angle to be determined. The optimum calibration fit uses an equation in Nusselt number, which is calculated from the Reynolds and Mach numbers using the Dewey correlation, and total temperature with calibration coefficients that are measured for every combination of flow angle. The calibration accuracy and repeatability are both good, yielding errors in flow parameters of approximately 2.7 % in Reynolds number, 5.4 % in Mach number and 2° in yaw angle. However, if not all the flow parameters are measured, there are significant extra errors in the Reynolds and Mach numbers due to necessary approximations about the flow field.

A complete theoretical analysis of the frequency response of a hot wire has shown that a correction is needed for experimental results at any frequency above approximately 1 Hz, without which significant errors will result. This correction is due to the presence of heat transfer by conduction. Above this frequency up to approximately 10 kHz, the sensitivity to heat transfer coefficient remains unchanged but the sensitivity to temperature drops to a constant value with negligible phase shift. A compensation factor has thus been derived for any hot wire that is solely dependent upon the overheat and heat transfer ratios.